Spectral representations of rough interface reverberation in stratified ocean waveguides

Henrik Schmidt
Massachusetts Institute of Technology
Cambridge, MA 02139

W.A. Kuperman*
Scripps Institution of Oceanography
La Jolla, CA 92093

An earlier developed perturbation approach to scattering from rough interfaces in stratified fluid-elastic media has been extended to provide a spectral representation of the higher-order statistics of waveguide reverberation, incorporating the combined physics of scattering and waveguide propagation. The formulation is compatible with existing propagation and ambient noise models based on wavenumber integration and therefore provides a more complete model with consistent treatment of all components of the acoustic environment. The model is used to demonstrate how reverberation affects the spatial correlation of the acoustic field, and the associated degradation in performance of high-resolution matched field processing approaches is discussed. In addition to the higher order statistics the formulation also provides a model for the reverberant field for specific roughness realizations, allowing for direct modeling of time-domain solutions, both in the spatial and the spectral domains, as illustrated by examples relevant to both deep and shallow water sonar scenarios.

PACS Subject Classification numbers 43.30Bp, 43.30Hw, 43.30Ma

INTRODUCTION

In this paper we extend previous work [1] to compute the reverberant field in a fluid-elastic waveguide with rough interfaces. The previous work developed a unified, self-consistent theory for predicting the effect of rough boundaries on the mean acoustic field in a fluid-elastic waveguide.

The structure of the reverberant field from boundary scattering in a waveguide must be studied using the combined physics of scattering from random interfaces and the same waveguide physics governing the mean field propagation. Further, since reverberation is, in effect, signal generated noise, the issue of signal extraction from noise and reverberation examined from a full wave theoretic point of view becomes of great interest. If one had a model of signal generated noise analogous to surface generated ambient noise [2, 3], then one could approach the signal processing in a manner analogous to previous matched field processing in correlated noise [4, 5]. Though all of these individual subjects, i.e., waveguide propagation, boundary scattering and matched field processing, have been extensively covered in the literature, the combination of the three remains a relatively unresearched area. One of the few examples is the work of Haralabus *et al.*[6] who used Monte-Carlo simulation of free surface scattering in a waveguide to analyze the effect of such environmental uncertainty on matched field processing.

Here, we develop a direct spectral representation of the reverberation statistics, providing a model of the signal-generated noise totally consistent with earlier developed models for the waveguide propagation[10] and ambient noise[3] components of the problem. As a result, we have developed a modeling framework which can be used to investigate the performance of both *passive* and *active* sonar processing concepts in ocean waveguides, based on consistent modeling of the whole seismo-acoustic environment.

The principal result of the previous work was the derivation of a boundary operator formulation using a perturbation approach which accounts for scattering at arbitrary fluid-elastic interfaces. When applied to a propagation theory or model like SAFARI it predicts the attenuation of the coherent component of the propagating acoustic fields, compressional and shear, as well as reflection and transmission coefficients of these fields at rough interfaces. The attenuation of the coherent fields arise from the generation of "scattered" compressional and shear waves in the stratification.

The theory was shown to contain the effects arising from coupling into evanescent waves unique to elastic media: Rayleigh (at vacuum-elastic interface), Scholte (at fluid-elastic interface) and Stoneley (elastic-elastic interface) waves.

The scattered fields were computed only for interfaces separating semi-infinite media whereas the coherent field

[1] Work initiated while at Naval Research Laboratory, Washington, DC 20375

computations were done for propagation in fully stratified complex waveguide. Numerical examples were shown to reproduce earlier work [7] using a different derivation. The results, however, shed further light on the problem of scattering at rough elastic interfaces in that its procedure clearly identifies the partitioning of scattered energy into compressional and shear body waves and evanescent waves. Furthermore, it was shown that an incident evanescent wave, in this case a Sholte wave, loses energy at a rough interface by scattering into homogeneous plane waves in the stratification.

The perturbation theory has later been combined with a model of random surface sources by Liu *et al.* [8] to provide a unified theory for rough bottom scattering of ambient noise in the ocean, demonstrating the significance of scattering into seismic modes in shaping the spectral behavior of the deep ocean noise field observed experimentally. LePage *et al.* [9] have used a full three dimensional implementation of the theory to model transmission loss in the Central Arctic, and based on excellent agreement with historical loss data, providing theoretical evidence for scattering into the flexural ice modes being the dominant loss mechanism in the Arctic.

We here extend the elastic perturbation theory to include a description of the scattered field as it is ultimately distributed in the waveguide environment responsible for its existence. Hence, the present approach provides a self-consistent method to compute reverberation in a waveguide.

We use the model to examine the spatial correlation structure of the reverberant field in a waveguide. Further, we demonstrate by a shallow water example how this modeling capability can be used to investigate the ultimate effect of the associated de-correlation of the total field on matched field processing.

We emphasize that the present reverberation model is far from being complete in terms of representing actual ocean environments. Thus, the environment is assumed to be range-independent. As a result discrete reverberation from environmental facets is not treated. Further, the model considers only rough interface reverberation. Clearly, other scattering mechanisms such as volume inhomogeneities may play an equally significant role in shaping the reverberant field. However, the objective of this work is not to produce a complete reverberation model for reproducing actual sonar scenarios, but rather to provide a consistent model of the signal, the ambient noise, and the reverberation in ocean waveguides.

Also, in terms of quantitative prediction, the present model is limited to diffuse reverberation from small-scale roughness. However, the physical implications of the coupling of the scattered field into the ocean waveguide are entirely general, at least in a qualitative sense, for arbitrary roughness characteristics.

As a final note, we stress that the present model does not implicitly distinguish between backward- and forward scattering. The results therefore apply to both passive and active sonar scenarios. Thus, the examples include narrow-band passive scenarios illustrating the effect of forward scattering on matched field processing performance. Clearly the time-envelope of the reverberation plays a significant role for active sonar performance, and to illustrate the capability of the present model in that regard we also include some broad-band results.

I. MATHEMATICAL FORMULATION

In the following we briefly review the main results of the perturbation theory for rough interface scattering in stratified elastic waveguides [1], and extend the formulation to provide a spectral representation of the spatial correlation of the reverberant waveguide field, compatible with existing wavenumber integration codes such as SAFARI [10].

A. Unperturbed stratified problem

The solution of the wave equation in horizontally stratified media by means of integral transforms or wavenumber integration is well established and forms the theoretical basis for several numerical models applied in seismology and underwater acoustics[11]. Only a brief outline of the features pertinent to the rough interface reverberation problem shall therefore be given at this point.

In a homogeneous and isotropic elastic medium, the seismo-acoustic field produced by one or more sources of time dependence $e^{j\omega t}$ can be expressed in terms of three scalar displacement potentials,

$$\chi_i(\mathbf{r},z) = \begin{cases} \phi_i(\mathbf{r},z), & \text{P waves} \\ \psi_i(\mathbf{r},z), & \text{SV waves} \\ \Lambda_i(\mathbf{r},z), & \text{SH waves .} \end{cases} \tag{1}$$

satisfying Helmholtz equations of the form

$$\nabla^2\chi + K^2(z)\chi = -\delta(\mathbf{r})\delta(z-z_s)\ , \tag{2}$$

In a fluid layer only the compressional potential $\phi_i(\mathbf{r},z)$ exists. Further, compressional sources only excite the P and SV potentials, eliminating the SH potential $\Lambda_i(\mathbf{r},z)$. Although most implementations involve only compressional sources all potentials are needed for the general scattering perturbation described below.

At the interfaces between layers i and $i+1$, the potentials must satisfy the boundary conditions of continuity of stresses and displacement, which can be stated in an operator form,

$$B_i(\chi_{i;i+1}) = 0, \quad i = 1,2,\ldots,N-1\ , \tag{3}$$

where N is the total number of layers, including the upper and lower halfspaces.

In a range-independent environment the Helmholtz equation can be Fourier transformed into the depth-separated wave equation

$$\frac{d^2\widetilde{\chi}}{dz^2} - [k^2 - k_i^2(z)]\widetilde{\chi} = -\frac{\delta(z-z_s)}{2\pi}, \tag{4}$$

with k_i being the wavenumber for compressional waves for the P potential $\phi(\mathbf{r},z)$ and the shear wavenumber for the

shear potentials. We express the solution to Eq. (4) as a superposition of a particular solution satisfying the inhomogeneous equation and a linear combination of the two independent homogeneous solutions. If the environment is decomposed into a stratification of isovelocity layers, the homogeneous solutions are exponentials and we obtain the following integral representation for the potentials in layer i.

$$\chi_i(\mathbf{r},z) = \frac{1}{2\pi}\int d^2\mathbf{k} e^{-j\mathbf{k}\cdot\mathbf{r}}\left[\widetilde{\chi}_i^-(\mathbf{k})e^{-jk_z z} + \widetilde{\chi}_i^+(\mathbf{k})e^{jk_z z}\right] , \tag{5}$$

where $k_z = \sqrt{k_i^2 - k^2}$, $k = |\mathbf{k}|$. Equation (5) can be interpreted as a plane wave decomposition of the field, with $\widetilde{\chi}^+(\mathbf{k})$ and $\widetilde{\chi}^-(\mathbf{k})$ being the amplitudes of upgoing and downgoing plane waves, respectively. The Fourier transform of the boundary conditions is

$$\widetilde{B}_i(\mathbf{k})\ \widetilde{\chi}^{\mp}_{i;i+1}(\mathbf{k}) = \widetilde{\mathbf{v}}_i(\mathbf{k}),\ \ i = 1,2,\ldots,N-1 \ , \tag{6}$$

with $\widetilde{\mathbf{v}}_i(\mathbf{k})$ being a vector containing the source contributions at interface i. Together with the radiation conditions for $z \to \pm\infty$, Eq. (6) defines a system of linear equations, the solution of which determines the unknown wavefield amplitudes $\widetilde{\chi}_i^{\mp}(\mathbf{k})$.

B. Rough Interface Perturbation

As demonstrated in the earlier paper, Ref. [1], elastic scattering by small scale roughness may be incorporated into the wavenumber integration formulation using a perturbational approach. Assume that the interface at depth z_i, separating the layers i and $i+1$ is not smooth, but rough with elevation $z - z_i = \gamma_i(\mathbf{r})$. The perturbation theory is valid for any particular, deterministic roughness realization, but in general the roughness will not be known in a deterministic sense. We therefore describe the roughness as a random process with mean zero, $\langle\gamma_i(\mathbf{r})\rangle = 0$. The roughness statistics are assumed to be homogeneous, defined through the spatial correlation function

$$N_i(\mathbf{r}'') = \langle\gamma_i(\mathbf{r})\gamma_i(\mathbf{r}')\rangle \ , \tag{7}$$

with $\mathbf{r}'' = \mathbf{r}' - \mathbf{r}$. $N_i(\mathbf{r}'')$ is the Fourier transform of the roughness power spectrum $P_i(\mathbf{p})$,

$$\langle\gamma_i^2\rangle P_i(\mathbf{p}) = \frac{1}{2\pi}\int d^2\mathbf{r}'' N_i(\mathbf{r}'')e^{-j\mathbf{p}\cdot\mathbf{r}''} \ . \tag{8}$$

The total field in layer number m is decomposed into a coherent or mean field $\langle\chi_m\rangle$ and an incoherent, scattered field, s_m,

$$\chi_m = \langle\chi_m\rangle + s_m \ . \tag{9}$$

Expansion of the total field about the mean interface now yields new sets of boundary conditions in the wavenumber domain, one for the *mean* field, and one for the *scattered* field.

Mean field

The first boundary condition derived in Ref. [1] concerns the amplitudes of the mean field, $\langle\chi\rangle$, at the average interface depth $z = z_i$,

$$\left[\widetilde{B}_i(\mathbf{k}) + \frac{\langle\gamma_i^2\rangle}{2}\frac{\partial^2}{\partial z^2}\widetilde{B}_i(\mathbf{k}) + I_1(\mathbf{k}) + I_2(\mathbf{k})\right]\langle\widetilde{\chi}^{\mp}_{i;i+1}(\mathbf{k})\rangle = 0 \ , \tag{10}$$

where the I_1 and I_2 are the scattering integrals [1]

$$I_1(\mathbf{k}) = -\frac{\langle\gamma_i^2\rangle}{2\pi}\int d^2\mathbf{q}\ P_i(\mathbf{q}-\mathbf{k})\frac{\partial\widetilde{B}_i(\mathbf{q})}{\partial z}\widetilde{T}_i(\mathbf{k},\mathbf{q}) \tag{11}$$

$$I_2(\mathbf{k}) = -\frac{\langle\gamma_i^2\rangle}{2\pi}\int d^2\mathbf{q}\ P_i(\mathbf{q}-\mathbf{k})\left[j(\mathbf{q}-\mathbf{k})\circ\widetilde{b}(\mathbf{q})\right] \times\widetilde{T}_i(\mathbf{k},\mathbf{q}) \ . \tag{12}$$

$\widetilde{T}_i(\mathbf{k},\mathbf{q})$ is the *T-matrix* for interface number i,

$$\widetilde{T}_i(\mathbf{k},\mathbf{q}) = \widetilde{B}_i^{-1}(\mathbf{q})\left[\frac{\partial\widetilde{B}_i(\mathbf{k})}{\partial z} - j(\mathbf{q}-\mathbf{k})\circ\widetilde{b}_i(\mathbf{k})\right] \ , \tag{13}$$

representing the transition between each mean field component of wavevector $\mathbf{k}$ in layers i and $i+1$ and the scattered components with wave vector $\mathbf{q}$ in the same layers, for unit roughness spectrum. The operation $\circ\widetilde{b}_i(\mathbf{k})$ represents the rotation of the boundary conditions on the rough surface [1].

By comparing Eqs. (6) and (10), it is clear that the effect of the rough surface scattering on the coherent field can be accounted for simply by replacing the original boundary conditions at interface i with the ones indicated in Eq. (10). Note that this operator formulation allows for simultaneous treatment of multiple rough interfaces. The perturbation theory is valid for $k_z\gamma_i \ll 1$ and $\gamma_i^{'} \ll 1$.

Whereas the boundary operator $\widetilde{B}_i(\mathbf{k})$ incorporates both the incident reflected and transmitted wavefield components, the selection of the boundary operator for the scattered field $\widetilde{B}_i(\mathbf{q})$ is more subtle. Thus, for a single interface separating two halfspaces, only outgoing components are present in accordance with the Rayleigh hypothesis. On the other hand, in waveguides the scattered field will be reflected at the other interfaces and return to the rough interface. In these cases it therefore becomes an issue whether these multiples should be included in the boundary operators for the scattered field. Here, the perturbation formulation assumes that the scattered field interacts incoherently with the mean field, but coherently with itself. To the first order this will only be the case if the multiples return to the rough interface within a range smaller than the roughness correlation length, which will only be the case if the other interfaces in the waveguide are close compared to the correlation length as well as the wavelength in the separating medium. For problems with thick layers only outgoing scattered components should therefore be included. On the other hand there are cases where multiples must be included. An example is the Arctic ice cover which is thin compared to the correlation length. As discussed by LePage *et al.* [9], the scattering into flexural modes is observed experimentally, and the excitation of these must therefore be included in the scattering integrals. Since these modes are the result of

constructive interference of exponentially growing and decaying waves in the ice cover, the surface multiples must be included in the boundary operator.

Reverberant field

To first order in the roughness the boundary conditions for the scattered field are [1]

$$\widetilde{B}_i(\mathbf{q})\widetilde{s}^{\mp}_{i;i+1}(\mathbf{q}) = -\frac{1}{2\pi}\int d^2\mathbf{k}\widetilde{\gamma}_i(\mathbf{q}-\mathbf{k}) \times \left[\frac{\partial \widetilde{B}_i(\mathbf{k})}{\partial z} - j(\mathbf{q}-\mathbf{k})\circ \widetilde{b}_i(\mathbf{k})\right]\langle\widetilde{\chi}^{\mp}_{i;i+1}(\mathbf{k})\rangle, \quad (14)$$

where $\mathbf{q}$ represents the wave vectors of the scattered Fourier components. Inserting Eq. (13) this equation can be written in the form,

$$\widetilde{s}^{\mp}_{i;i+1}(\mathbf{q}) = -\frac{1}{2\pi}\int d^2\mathbf{k}\widetilde{\gamma}_i(\mathbf{q}-\mathbf{k})\widetilde{T}_i(\mathbf{k},\mathbf{q})\langle\widetilde{\chi}^{\mp}_{i;i+1}(\mathbf{k})\rangle, \quad (15)$$

which makes it clear why $\widetilde{T}_i(\mathbf{k},\mathbf{q})$ physically represents a *transition* or *coupling* matrix between coherent field components with wavevector $\mathbf{k}$ and scattered components of wavevector $\mathbf{q}$. However, since the matrix inversion $\widetilde{B}_i(\mathbf{q})$ is independent of the integration variable, the form in Eq. (14) is computationally more efficient. This equation was used by Kuperman and Schmidt [1] to compute the *scattering kernel* $\widetilde{s}^{\mp}_{i;i+1}(\mathbf{q})$ for plane waves incident on an interface separating two infinite halfspaces, involving only outgoing scattered components. However, we can straightforwardly use Eq. (14) to compute waveguide reverberation including all multiples, modes etc. This is clear from simply observing that Eq. (14) is of the same form as the unperturbed equation (6), but with the source contribution on the right hand side replaced by an integral over all mean field wavenumber components. For a particular roughness realization $\gamma_i(\mathbf{r})$ this integral can therefore be interpreted physically as representing a virtual source distribution at the rough interface depth. The reverberant field generated by these virtual sources will clearly propagate according to the same waveguide physics as the mean field, including transmission and reflection at all interfaces and the formation of normal modes. This propagation behavior of the reverberant field is incorporated simply by replacing the *local* boundary operator on the left hand side of Eq. (14) with the *global* boundary operator including all interfaces in the stratification. The resulting equation for the wavenumber spectrum of the reverberant field is therefore,

$$\widetilde{B}_i(\mathbf{q})\widetilde{s}^{\mp}_{i;i+1}(\mathbf{q}) = \mathbf{f}_i(\mathbf{q}) \quad , i = 1,\ldots,N-1\,, \quad (16)$$

where the vector $\mathbf{f}_i(\mathbf{q})$ represents the wavenumber integral on the right hand side of Eq. (14). In the waveguide the reverberant field will obviously *re-scatter* when interacting with the rough interfaces. Use of the smooth boundary boundary operator will therefore *over-estimate* the amplitudes of the reverberant field. However, in analogy to the mean field, this re-scattering is easily incorporated by using the perturbed boundary operator in Eq. (10), instead of the smooth one, i.e.

$$\widetilde{B}^*_i(\mathbf{q})\widetilde{s}^{\mp}_{i;i+1}(\mathbf{q}) = \mathbf{f}_i(\mathbf{q}) \quad , i = 1,\ldots,N-1\,, \quad (17)$$

where the perturbed boundary operator $\widetilde{B}^*_i$ is defined in Eq. (10). Equation (17) obviously eliminates the *re-scattered* components from the total scattered field and therefore *under-estimates* the scattered field amplitudes. As a result, Eqs. (16) and (17) provide upper and lower bounds for the scattered field intensity. On the other hand the higher order of the approximation suggests that Eq. (17) will be closest to the correct answer for most waveguide problems with realistic penetrable bottoms.

Once the mean field is found, Eq. (16) may be solved using the standard methods [11], and the scattered field in layer m follows using the Fourier transform, Eq. (5),

$$s_m(\mathbf{r},z) = \frac{1}{2\pi}\int d^2\mathbf{q}e^{-j\mathbf{q}\cdot\mathbf{r}}\widetilde{s}^{\mp}_m(\mathbf{q})e_m(\mathbf{q},z)\,. \quad (18)$$

where $e_m(\mathbf{q},z)$ is a diagonal matrix representing the exponential behavior of the up- and downgoing plane wave components in layer m.

Interpretation of reverberation data is often performed using array processing to reveal its angular or spectral distribution. Here, the present theory inherently computes the frequency-wavenumber $(\omega-k)$ response directly in the form of the scattering kernel $\widetilde{s}^{\mp}_m(\mathbf{q})e_m(\mathbf{q},z)$, but can also be applied to compute the time-domain $\tau-p$ equivalent[13], with τ being the vertical intercept time and p being the horizontal slowness. Thus, it is easily shown that the $\tau-p$ response is obtained by simply eliminating the wavenumber integral in Eq. (18), but only performing the Fourier syntheses of components of equal horizontal slowness vector $\mathbf{p}$,

$$s_m(\mathbf{p},\tau) = \frac{1}{2\pi}\int d\omega e^{j\omega\tau}\widetilde{s}^{\mp}_m(\omega\mathbf{p})e_m(\omega\mathbf{p},z)\,. \quad (19)$$

In the examples following we will give examples of full time-domain responses in both the spatial and the $\tau-p$ domains.

Reverberation statistics

Equations (16) and (18) can be used to model the scattered field for specific roughness realizations, but in general only the roughness statistics will be known, e.g. through the spatial spectrum $P_i(\mathbf{k})$. In such cases, however, we can derive an expression for the spatial correlation function for the reverberant field,

$$C_S(\mathbf{r}_1,z_1,\mathbf{r}_2,z_2) = \langle s_m(\mathbf{r}_1,z_1)s^{\dagger}_n(\mathbf{r}_2,z_2)\rangle\,, \quad (20)$$

where m and n are the layers including the two receivers, and the $\dagger$ represents the complex conjugate. Insertion of Eq. (18) yields

$$C_S(\mathbf{r}_1,z_1,\mathbf{r}_2,z_2) = = \frac{1}{(2\pi)^2}\int\int d^2\mathbf{q}_1 d^2\mathbf{q}_2 e^{-j(\mathbf{q}_1\cdot\mathbf{r}_1-\mathbf{q}_2\cdot\mathbf{r}_2)} \times e_m(z_1,\mathbf{q}_1)e^{\dagger}_n(z_2,\mathbf{q}_2)\langle\widetilde{s}_m(\mathbf{q}_1)\widetilde{s}^{\dagger}_n(\mathbf{q}_2)\rangle\,. \quad (21)$$

Inserting Eqs. (16), and using the identity

$$\frac{1}{2\pi}\int d^2\mathbf{r}e^{j\mathbf{k}\cdot\mathbf{r}} = \delta(\mathbf{k}) \ , \tag{22}$$

and Eq. (8), we arrive after some algebra at the following expression for the correlation function of the reverberation from the rough interface i,

$$C_S(\mathbf{r}_1, z_1, \mathbf{r}_2, z_2) = \frac{\langle\gamma_i^2\rangle}{(2\pi)^3}\int d^2\mathbf{p}P_i(-\mathbf{p})\left[\int d^2\mathbf{q}A_m(z_1,\mathbf{q},\mathbf{q}+\mathbf{p})e^{-j\mathbf{q}\cdot\mathbf{r}_1}\right] \times\left[\int d^2\mathbf{q}A_n(z_2,\mathbf{q},\mathbf{q}+\mathbf{p})e^{-j\mathbf{q}\cdot\mathbf{r}_2}\right]^\dagger \tag{23}$$

with

$$A_m(z,\mathbf{q},\mathbf{k}) = e_m(z,\mathbf{q})\widetilde{T}^*_{i;m}(\mathbf{k},\mathbf{q})\langle\widetilde{\chi}^{\mp}_{i;i+1}(\mathbf{k})\rangle \ , \tag{24}$$

Here, $\widetilde{T}^*_{i;m}(\mathbf{k},\mathbf{q})$ is the *reverberation T-matrix* representing the transition from mean field components with wave vector $\mathbf{k}$ in the layers separated by interface i, and the reverberation components of wave vector $\mathbf{q}$ in layer m. It is defined by an expression similar to Eq. (13), but with the local boundary operator $\widetilde{B}_i(\mathbf{q})$ replaced by the global operator, or the perturbed operator $\widetilde{B}^*_i(\mathbf{q})$, $i = 1,\ldots,N-1$. Using the same perturbation theory, an expression similar to Eq. (23) was derived by Goalwin [12] for the correlation of the scattered field in a fluid halfspace with a rough pressure release surface. However, the operator form in Eq. (23) is entirely general in terms of waveguide stratification including fluid as well as elastic layers.

II. NUMERICAL IMPLEMENTATION

The operator formalism derived above for both the mean and the reverberant fields are entirely general in terms of two-dimensional roughness statistics, and does not make any assumptions concerning horizontal isotropy. Thus, LePage *et al.* [9] made a full implementation of the coherent field equation (10), incorporating 3-D scattering from an Arctic ice cover with anisotropic roughness statistics. They found only a minor effect of 3-D scattering on the coherent field, but demonstrated the strong 3-D nature of the scattering kernel, suggesting that out-of-plane scattering is important for modeling the reverberant field. Liu *et al.* [8] also demonstrated the inherent 3-D nature of the scattered field in fluid-elastic stratifications, using the present perturbation theory to model sea-bed scattering of surface-generated ambient noise.

Also, it should be stressed that the expressions represent both mono- and bi-static reverberation, including both *forward* and *backward* scattering.

Unfortunately, the evaluation of the two-dimensional integrals in Eq. (23) are computationally intensive, in particular for waveguides, due to the wavenumber sampling requirements (see e.g. Ref. [11], Sec. 4.5). On the other hand, the evaluation of spectral representations are extremely well suited for implementation on modern massively parallel computers, such as done by LePage *et al.* [9]. Even though the evaluation of Eq. (23) is therefore not prohibitive on such computer architectures, we will here limit ourselves to demonstrate the use of the operator formulations to two-dimensional scenarios. We do that for primarily two reasons. First of all the 2-D modeling is adequate for demonstrating the significance of the waveguide physics in shaping the reverberant field, which is the primary scope of this paper. Secondly a 2-D implementation allows us to use the existing SAFARI code [10] with rather simple modifications to evaluate the spectral representations of the reverberant field.

As a first step we use the standard SAFARI code, which has the perturbed boundary conditions in Eq. (10) implemented, to evaluate the coherent component of the field, but also outputting the vectors $\partial\widetilde{B}_i(\mathbf{k})/\partial z\langle\widetilde{\chi}^{\mp}_{i;i+1}(\mathbf{k})\rangle$ and $\widetilde{b}_i(\mathbf{k})\langle\widetilde{\chi}^{\mp}_{i;i+1}(\mathbf{k})\rangle$, representing the virtual source distributions at the rough interfaces. These are then input to special versions of SAFARI with the physical sources replaced by the virtual sources.

One version computes realizations of the reverberant field by generating random realizations of the roughness spectrum $\widetilde{\gamma}_i(\mathbf{p})$. Then, for each value of the scattered wavenumber $\mathbf{q}$, the wavenumber integral in Eq. (14) is evaluated numerically, and the resulting global equation (16) is then solved using the existing SAFARI direct global matrix kernel. The inverse transform is performed in the standard way either by evaluating the 1-D Fourier transform for plane problems or by a Hankel transform for problems with cylindrical symmetry [10, 11], followed by Fourier synthesis for time-domain solutions [11]. This approach is computationally very efficient, with computation times almost identical to those involved in evaluating the mean field.

Another, slightly more complex version of SAFARI is used for computing the correlation function in Eq. (23). Here, the kernels $A_m(z,\mathbf{q},\mathbf{q}+\mathbf{p})$ are evaluated for all values of $\mathbf{q}$ in a way which is basically identical to the one described above, but taking advantage of the fact that the same global matrix inversion is used for all values of $\mathbf{p}$. All spectral integrals are then evaluated in the standard way, yielding the covariance matrix for an arbitrary receiver array. The diagonal elements represent the expectation value of the reverberant field intensity at each receiver.

In the earlier paper [1] we used a Gaussian roughness spectrum, but since the choice of spectrum is arbitrary we will here use a more realistic, one-dimensional Goff-Jordan [14] power law spectrum:

$$P(p) = \pi L\left((pL)^2+1\right)^{-1.5} \ , \tag{25}$$

where L is a charactistic correlation length.

III. NUMERICAL EXAMPLES

A. Deep water bottom reverberation

The first example concerns a scenario representing the 1992 experiment carried out in the mid-Atlantic under the

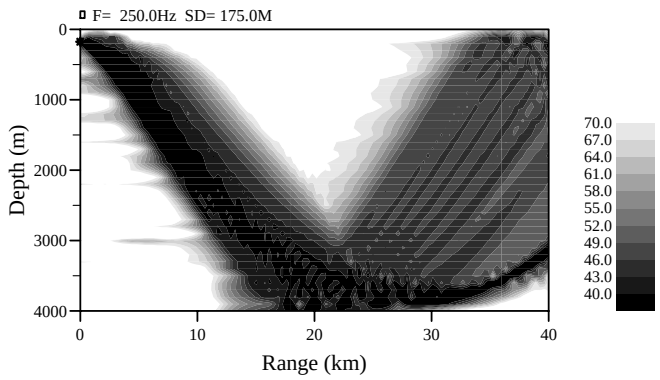

Figure 1: Contours in dB of coherent transmission loss for ARSRP scenario. The bottom is insonified by a vertical array of 11 sources steered downward at a nominal grazing angle of 6°. Plane geometry.

Acoustic Reverberation Special Research Program (ARSRP). Even though the present model does not represent the strongly range-dependent bathymetry of the actual ARSRP experiment, we will use this experimental scenario to illustrate how the spatial and temporal distribution of deep ocean bottom reverberation is a combined effect of the scattering process and the waveguide physics. In other words it is not the intention here to model the actual experimental data. We assume the environment to be range-independent with a water depth of 4000 m, with a sound speed profile measured during the experiment. The bottom is assumed to be rough with a Goff-Jordan power spectrum, Eq. (25). The RMS height is assumed to be 2 m and the correlation length is variable. A vertical source array with 11 elements was used to insonify the bottom at low grazing angles in half a convergence zone. The source was emitting wideband pulses with approximate center frequency 250 Hz and bandwidth 100 Hz. For the source array steered downward 6° grazing, the transmission loss predicted by SAFARI for this scenario is shown in Fig. 1. We assumed plane geometry, with the effect of removing the cylindrical spreading loss in the predictions. The depth-range contours of the transmission loss illustrate the wide spectral nature of the beam, giving rise to strong interference effects in the insonified area as well as in the reflected field.

Figure 2 shows the expectation value of the reverberant field intensity, computed using Eq. (23) for two different correlation lengths, (a) $L = 50$ m, (b) $L = 6$ m. The spatial distribution of the reverberant field is clearly dependent on the roughness correlation length. For $L = 50$ m the roughness slopes are small, and the scattered field becomes highly specular, with insignificant mono-static reverberation as a result. In contrast the $L = 6$ m has many roughness features of wavelength size, and larger slopes, leading to a both stronger scattering and a wider spectral spreading, including negative wavenumbers, with the effect of significantly increasing the mono-static reverberation.

This dependency of the spectral spreading on the correlation length is consistent with the form of Eq. (23).

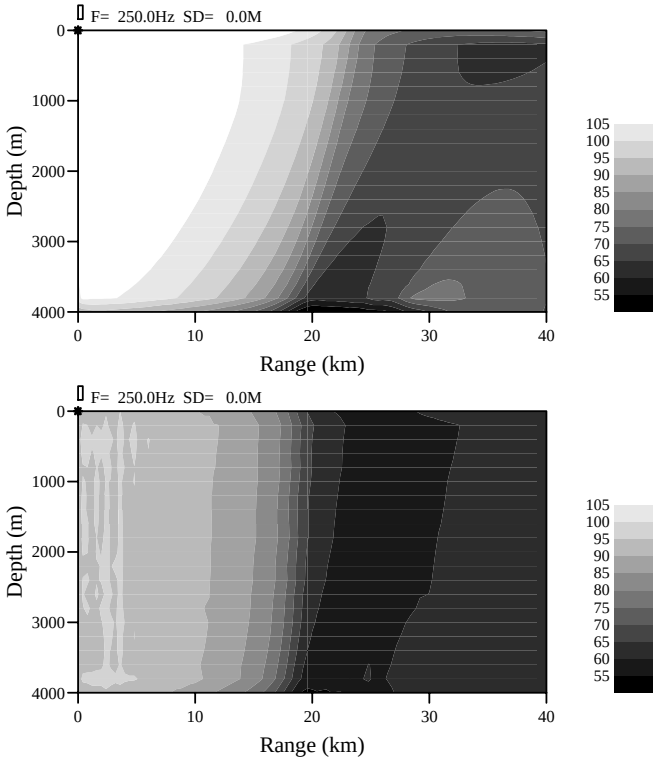

Figure 2: Contours in dB of expectation value of the scattered field intensity for ARSRP scenario. A one-dimensional Goff-Jordan roughness spectrum is assumed, with RMS-elevation 2 m. (a): Correlation length 50 m. (b): Correlation length 6 m.

Thus, a short correlation length corresponds to a wide spectrum $P(\mathbf{p}) = P(\mathbf{q} - \mathbf{k})$, allowing an incoming wave of wavenumber $\mathbf{k}$ to scatter into a wide spectrum of wavenumbers $\mathbf{q}$.

Figure 3 shows a time domain realization of the mean and scattered fields as observed on a vertical array just above the seabed. For simplicity we here assume that the incoming field consists of a single plane wave component with grazing angle 5°. The vertical array is 100 m long, with a total of 50 receivers with the lowermost 2 m above the seabed. The incident field is a transient with center frequency 250 Hz and 100 Hz bandwidth. The mean field as observed on the array is shown in Fig. 3(a), exhibiting the expected vertical interference pattern. Fig. 3(b) shows the scattered field observed by the array as computed using Fourier synthesis of solutions to Eq. (16). The strongest components of the scattered field are directly interfering with the mean field at time $t = 0$. This reverberation is associated with "upstream" *forward scattering*. The later reverberation arrivals are due to "downstream" *backscattering*. Note the limited spatial correlation of the scattered field. A particularly interesting feature is the relatively low reverberation immediately following the mean field. A Lambert's law behavior would suggest a gradual decrease in reverberation following the mean field arrival. This suggests that the spectral composition of the scattered field from the elastic granite interface does not have a maximum at the vertical such as predicted by Lambert's

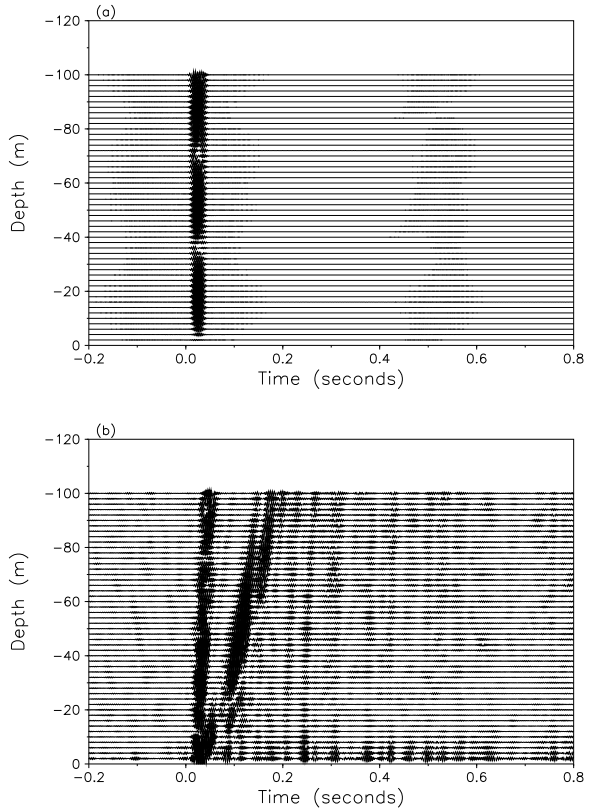

Figure 3: Time-domain response on vertical array in water halfspace overlying a granite bottom. The rough seabed has 2 m RMS excursion and a Goff-Jordan power spectrum with correlation length 6 m. A plane wave is incident at 5° grazing on the bottom, with a transient pressure pulse of center frequency 250 Hz and bandwidth 100 Hz. (a): Coherent field. (b): Scattered field.

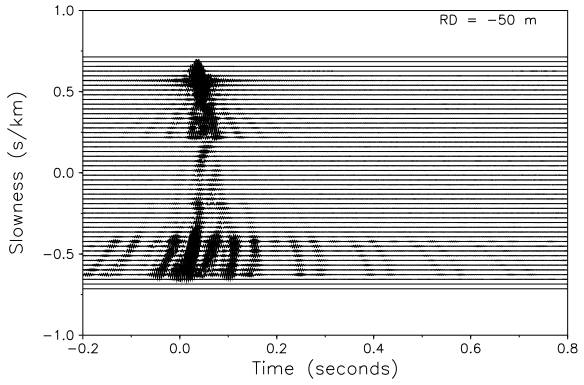

Figure 4: $\tau - p$ representation of scattered field at depth 50 m above rough granite bottom.

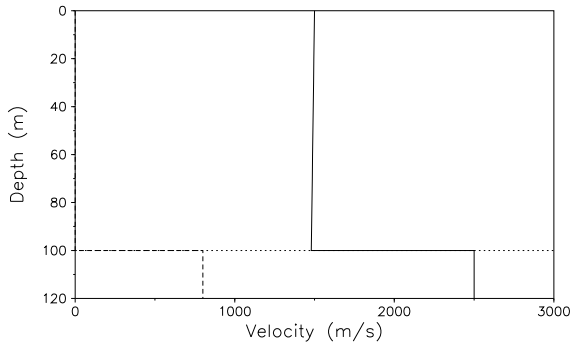

Figure 5: Shallow water environment with downward refracting sound speed profile and a randomly rough limestone bottom

law, but rather has a quadrapole behavior with maxima in a forward and a backward directions. As described above this hypothesis can be directly verified by computing the scattered field in the $\tau - p$ domain, Eq. (19). This is done in Fig. 4, showing the $\tau - p$ response computed for a depth 50 m above the rough interface. Negative slowness corresponds to backscattering, and positive slowness to forward scattering. In this representation it is clear, that the low level of small slowness scattering is associated with the grazing angles being larger than critical for the bottom. At these slownesses most of the scattered energy is apparently radiating into the bottom. This non-Lambert scattering behavior of the elastic interface has also been demonstrated by Levander *et al.* using finite difference modeling [16].

Another interesting phenomenon is the strong scattering into evanescent Scholte waves, observable on the sensors close to the bottom. The Scholte waves propagate along the interface with phase- and group velocity slightly less than the speed of sound in water, and as a result, the time-spread of these arrivals is significant. Some of the discrete Scholte wave arrivals are clearly associated with arrivals visible also on the upper receivers. These arrivals are due to backscattering from bottom features "downstream".

B. Shallow water reverberation

As a second example we consider the shallow water environment shown in Fig. 5. The water depth is 100 m, and the sound speed profile is downward refracting, with 1500 m/s at the surface and 1480 m/s at the seabed. The bottom is assumed to be an infinite halfspace of limestone with compressional speed 2500 m/s and shear speed 800 m/s. The compressional and shear attenuations are 0.1 and 0.2 db/λ, respectively, and the density is 2200 kg/m^3. The seabed is randomly rough with a Goff-Jordan power spectrum and an RMS excursion of 1 m.

Figure 6 shows contours in depth and range of the mean field transmission loss in dB. The correlation length of the bottom roughness is 10 m. The downward refracting profile has the effect of rapidly attenuating the higher or-

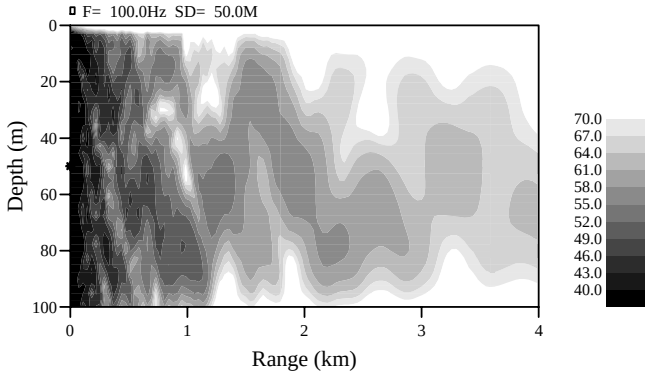

Figure 6: Contours in dB of coherent transmission loss for a 100 Hz point source at depth 50 m in shallow water environment.

der modes, leaving a relatively simple interference pattern beyond a range of a couple of km.

Figure 7 shows the transmission loss as well as the expectation value of the reverberation intensity vs range at mid water depth. The solid curves represent the mean field, whereas the dashed and dotted curves show the reverberation intensity for 10 m and 100 m correlation length, respectively. In Fig. 7(a) the scattered field intensity was computed using the unperturbed boundary operator, Eq. (16), whereas in Fig. 7(b) the perturbed boundary operator in Eq. (17) was used. Note here that the expectation value for the reverberant intensity is largest for the long correlation length. This may seem surprising in view of the fact that the scattering loss is larger for the short correlation length. The reason for this behavior is that the longer correlation length produces virtual sources of higher spatial coherence than the finer scale roughness, and therefore provide a stronger excitation of the normal modes of the waveguide.

Note also that the re-scattering of the reverberation creates the same modal stripping as observed for the mean field, although somewhat delayed in range, as expected, yielding a modal interference pattern very similar to the one of the coherent field.

More important to high resolution array processing than coherent loss is the reduction in spatial correlation created by the reverberant field. This property is again directly modeled using Eq. (23). Figures 8 and 9 show the normalized vertical correlation and coherence at 4 km for two different reference depths, 25 and 75 m. We use the following definition of the normalized correlation,

$$C_{ij} = \frac{\mathrm{Re}[C_S(\mathbf{r}_i, z_i, \mathbf{r}_j, z_j)]}{\sqrt{C_S(\mathbf{r}_i, z_i, \mathbf{r}_i, z_i) C_S(\mathbf{r}_j, z_j, \mathbf{r}_j, z_j)}} , \qquad (26)$$

and for the coherence,

$$\rho_{ij}^2 = \frac{|C_S(\mathbf{r}_i, z_i, \mathbf{r}_j, z_j)|^2}{C_S(\mathbf{r}_i, z_i, \mathbf{r}_i, z_i) C_S(\mathbf{r}_j, z_j, \mathbf{r}_j, z_j)} . \qquad (27)$$

The dotted curves show the results for the coherent field, whereas the dashed curves indicate the correlation and coherence of the scattered field. The solid curves represent the resulting expectation value of the correlation and

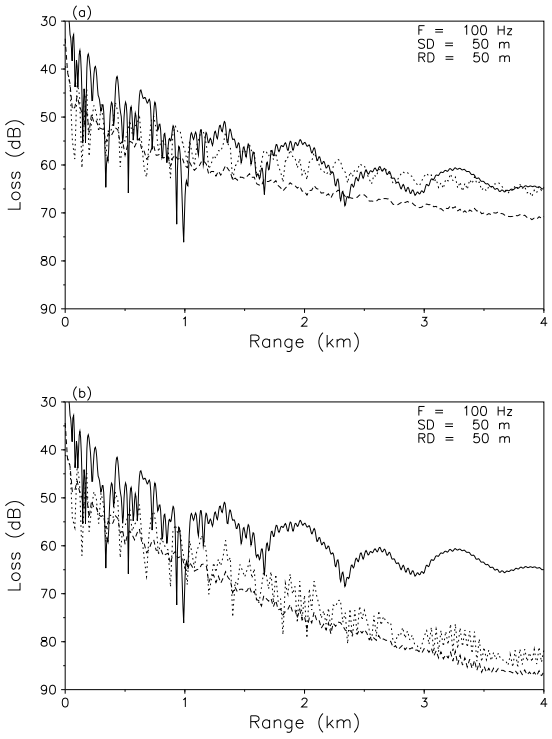

Figure 7: Mean field transmission loss and expectation value of scattered field at 100 Hz for receiver at 50 m depth in shallow water waveguide with limestone bottom with 1m RMS roughness. Solid curves indicate mean field for 10 m correlation length. The dashed and dotted curves show the expectation value of the scattered field intensity for 10 and 100 m correlation lengths, respectively. Scattered field intensity computed using (a): the unperturbed boundary operator; (b): the perturbed boundary operator.

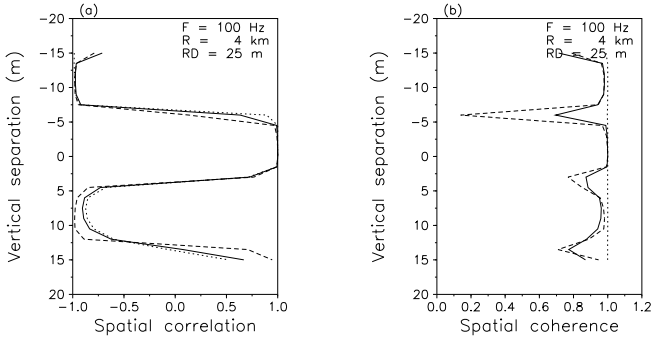

Figure 8: Spatial correlation of acoustic field at 100 Hz on vertical array of 30 m length, with the center receiver at 25 m depth. The source is at depth 50 m and range 4 km. (a) Normalized spatial correlation. (b) Spatial coherence.

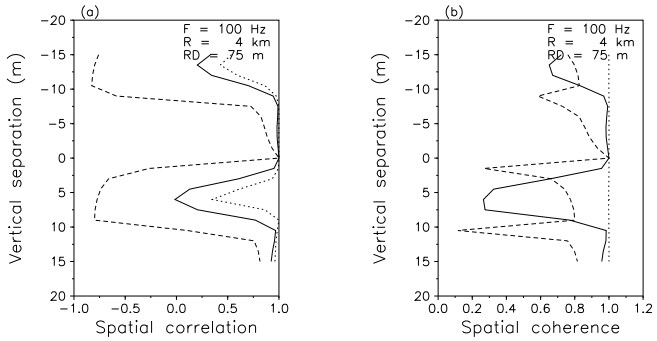

Figure 9: Spatial correlation of acoustic field at 100 Hz on vertical array of 30 m length, with the center receiver at 75 m depth. The source is at depth 50 m and range 4 km. (a) Normalized spatial correlation. (b) Spatial coherence.

coherence of the total field. Clearly, the effect of roughness scattering on the spatial correlation is most significant close to the rough bottom.

The effect of the decorrelation on high resolution array processing is illustrated in Fig. 10. A maximum likelihood matched field processor [4] is used on a vertical array spanning the whole water column to localize a point source at mid water depth and 4 km range. The matched field replicas assume a smooth bottom, and Fig. 10(a) shows the MFP ambiguity function for the case where the field covariance matrix is generated assuming a smooth bottom as well, clearly identifying a sharp peak at the correct source position. Figure 10(b) shows the ambiguity function obtained when the covariance matrix for the reverberant field produced by a roughness with $L = 10m$ is added to the mean field covariance matrix. The associated decorrelation has the effect of adding a number of false source positions in the ambiguity function, even though, for this relative small roughness, the largest peak still appears in the right position.

Finally, to illustrate the temporal distribution of the waveguide reverberation, we present in Fig. 11 the time domain results for a realization of the $L = 10m$ roughness. The source emits a transient pulse with center frequency 100 Hz and bandwidth 100 Hz. Fig. 11(a) shows the coherent component on a 9-element vertical array at 1 km range. Even though the field is dominated by the fast lower order modes, some later, high mode number arrivals are observed. Fig. 11(b) shows the superposition of the coherent and the scattered fields. We here ignored rescattering by using the unperturbed boundary operator, Eq. (16), and as expected from Fig. 7(a), the scattering significantly increases the amplitude of the late modal arrivals.

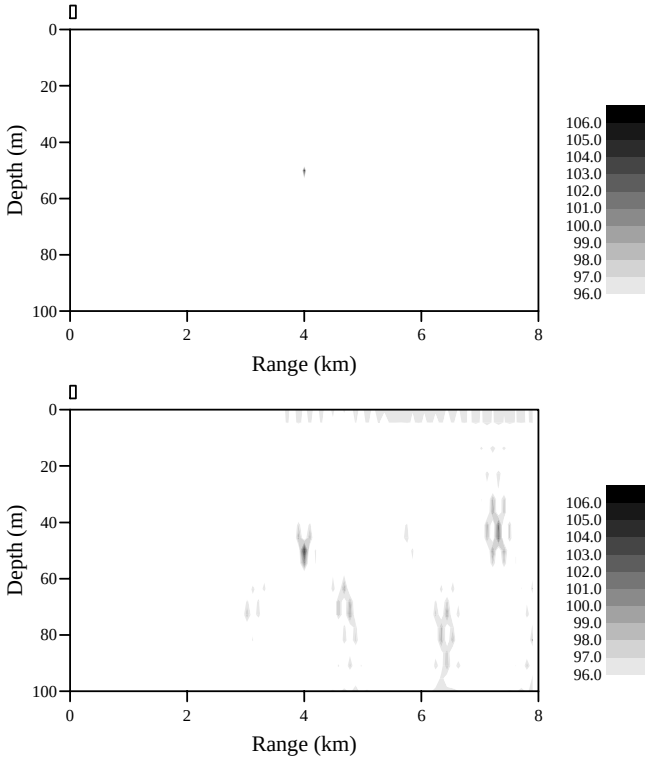

Figure 10: Maximum Likelihood ambiguity function in dB for matched field source localization in shallow water environment. A 100 Hz source of level 160 dB is present at 50 m depth and range 4 km from vertical array spanning the whole water column. A correlated ambient noise field is generated by a distribution of surface sources of strength 50 dB, yielding an average noise level of 56 dB. (a) Smooth bottom. (b) Rough bottom.

C. Arctic ice reverberation

As demonstrated by LePage *et al.* [9] the scattering perturbation approach performs excellently in reproducing the measured coherent transmission loss in the Arctic, in spite of the fact that it only represents the prominent,

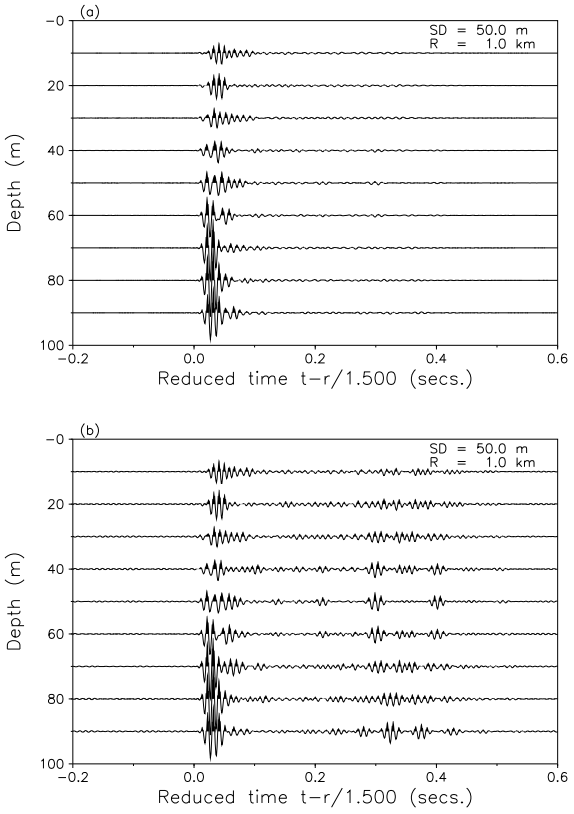

Figure 11: Time-domain response on vertical array at 1 km range in shallow water environment. The limestone bottom has 1 m RMS roughness and a Goff-Jordan power spectrum with correlation length 10 m. The source is at 50 m depth, transmitting a Hanning weighted sine pulse with center frequency 100 Hz and bandwidth 100 Hz. (a): Mean field. (b): Total field.

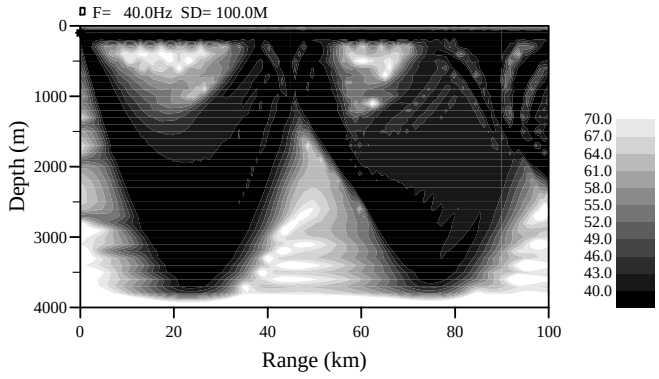

Figure 12: Contours of transmission loss in dB at 40 Hz in Central Arctic environment. The source is at depth 100 m. Plane geometry.

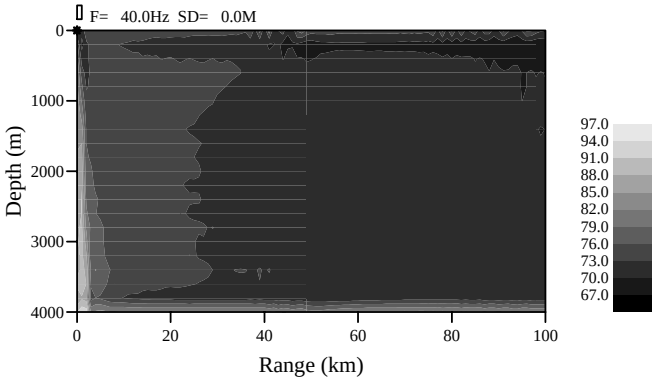

Figure 13: Contours of expectation value of scattered field in dB at 40 Hz in Central Arctic environment. Plane geometry.

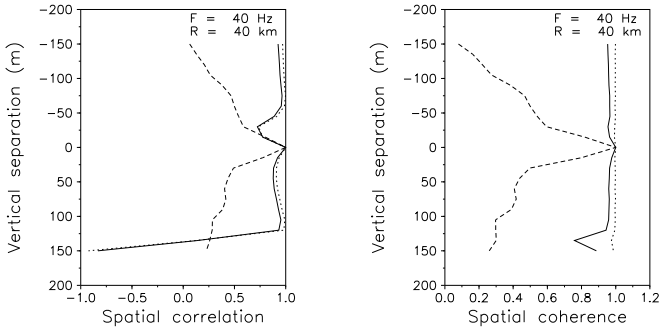

Figure 14: Spatial correlation properties of acoustic field at 40 Hz on vertical array of 300 m length, with the uppermost receiver at 15 m depth. The source is at depth 100 m and range 40 km. (a) Normalized spatial correlation. (b) Normalized spatial coherence.

discrete ice keels in an average spectral sense. We therefore expect the present spectral representation to provide a realistic model for the reverberant field as well. The typical Arctic transmission loss is shown in the form of contours vs depth and range in Fig. 12. The frequency is 40 Hz and the source depth is 100 m. The contours clearly show the separation into the surface duct propagation and the CZ paths. Since all propagation paths interact with the ice cover, the spatial correlation of the field is governed almost entirely by the irregularity of the ice cover, including the roughness [15]. This property is directly modeled using Eq. (23). Thus, Fig. 13 shows the expectation values of the scattered field intensity vs depth and range for an ice cover with 2 m RMS roughness and correlation length 40 m. For clarity we have removed the cylindrical spreading. It is interesting to note how more and more scattered (incoherent) energy gets trapped in the surface channel after each CZ. Even though we here used the unperturbed boundary operator in Eq. (23), this phenomenon suggests that the spatial correlation vs depth may provide a usuable acoustic signature of changes in ice roughness, relevant to acoustic monitoring of climatic changes in the Arctic[17]. Fig. 14 shows the computed correlation and coherence on a vertical array spanning the surface channel at 40 km range. The dotted line shows the correlation of the field without roughness. The coherence of the mean field is imperfect due to the fact that a realistic correlated noise field is included [3]. The dashed line shows the correlation of the scattered field, and the solid curve shows the result for the total field. Note the inhomogeneity of the correlation introduced by the different modal penetration depths.

IV. CONCLUSIONS

Using an earlier developed perturbation approach to scattering from rough interfaces in stratified fluid-elastic media, a spectral representation of the higher-order statistics of waveguide reverberation has been derived. The formulation is compatible with existing propagation and ambient noise models based on wavenumber integration and therefore provides a more complete model with consistent modeling of all components of the acoustic environment. The model has been used to demonstrate how reverberation affects the spatial correlation of the acoustic field, and the associated performance degradation of high-resolution matched field processing has been discussed. In addition to the higher order statistics the formulation also provides a model for the reverberant field for specific roughness realizations, allowing for direct modeling of time-domain solutions, both in the spatial and the spectral domains, as illustrated by examples relevant to both deep and shallow water sonar scenarios.

Acknowledgements

This work was supported by the Office of Naval Research, in part by the Acoustic Reverberation Special Research Program (ARSRP), the Ocean Acoustics and the High Latitude Dynamics programs.

References

[1] W.A. Kuperman and H. Schmidt. Self-consistent perturbation approach to rough surface scattering in stratified elastic media. *J. Acoust. Soc. Am.*, **86**, 1511–1522 (1989).

[2] W.A. Kuperman and F. Ingenito. Spatial correlation of surface generated noise in a stratified ocean. *J. Acoust. Soc. Am.*, **67**, 1988–1996 (1980).

[3] H. Schmidt and W.A. Kuperman. Estimation of surface noise source level from seismo-acoustic ambient noise measurements. *J. Acoust. Soc. Am.*, **84**, 2153–2162 (1988).

[4] A.B. Baggeroer, W.A. Kuperman and H. Schmidt. Matched field processing: Source localization in correlated noise as an optimum parameter estimation problem. *J. Acoust. Soc. Am.*, **82**, 571–587 (1988).

[5] A.B. Baggeroer, W.A. Kuperman and P.N. Mikhalevsky. An overview of matched field methods in ocean acoustics. *IEEE J. Oceanic Eng.*, **18**, 401–424 (1993).

[6] G. Haralabus, V. Premus, D. Alexandrou, L.W. Nolte, and A.M. Richardson. Source localization in uncertain acoustics scattering environment. *J. Acoust. Soc. Am.*, **94**, 3379–3386 (1993).

[7] D.K. Dacol and D.H. Berman. Sound scattering from a randomly rough fluid-solid interface. *J. Acoust. Soc. Am.*, **84**, 292–302 (1988).

[8] J.-Y. Liu, H. Schmidt, and W.A. Kuperman. Effect of a rough seabed on the spectral composition of deep ocean infrasonic ambient noise. *J. Acoust. Soc. Am.*, **93**, 753–769 (1993).

[9] K. LePage and H. Schmidt. Modeling of low frequency transmission loss in the central Arctic. *J. Acoust. Soc. Am.*, **96**, 1783–1795 (1994).

[10] H. Schmidt. SAFARI: Seismo-acoustic fast field algorithm for range independent environments. user's guide. SR 113, SACLANT ASW Research Centre, La Spezia, Italy, 1987.

[11] F.B. Jensen, W.A. Kuperman, M.B. Porter, and H. Schmidt. *Computational Ocean Acoustics*. American Institute of Physics, New York, 1994.

[12] P.W. Goalwin. A stationary phase approach to the calculation of the acoustic field scattered from a two-dimensional random sea surface. *J. Acoust. Soc. Am.*, **93**, 214–223 (1993).

[13] M. Dietrich. Modeling of marine seismic profiles in the $t-x$ and $\tau-p$ domains. *Geophysics*, **53**, 453–465 (1988).

[14] J. Goff and T. Jordan. Stochastic modeling of seafloor morphology: inversion of sea beam data for second order statistics. *J. Geophys. Res.*, **93**, 13589–13608 (1988).

[15] K.D. LePage. *Elastic scattering in oceanic waveguides*. PhD thesis, Massachusetts Institute of Technology, September 1992.

[16] A. Levander, A. Harding and J. Orcutt. Numerical scattering results for a rough, unsedimented seafloor. In *Ocean Reverberation*, Ed. D.D. Ellis, J.R. Preston and H.G. Urban, Kluwer Academic Publishers, Dordrecht, The Netherlands (1993).

[17] P.N. Mikhalevsky, Feasibility of acoustic thermometry of Arctic Ocean climate change, *J. Acoust. Soc. Am.*, **94**(3), 1760 (1993).